AAC
Journals.ASM.org

Structural and Inhibition Studies of the RNase H Function of Xenotropic Murine Leukemia Virus-Related Virus Reverse Transcriptase

Karen A. Kirby,[a,b] Bruno Marchand,[a,b] Yee Tsuey Ong,[a,b] Tanyaradzwa P. Ndongwe,[a,b] Atsuko Hachiya,[a,b] Eleftherios Michailidis,[a,b] Maxwell D. Leslie,[a,b] Daniel V. Sietsema,[a,b] Tracy L. Fetterly,[a,b] Christopher A. Dorst,[a,b] Kamalendra Singh,[a,b] Zhengqiang Wang,[c] Michael A. Parniak,[d] and Stefan G. Sarafianos[a,b,e]

Christopher S. Bond Life Sciences Center, University of Missouri, Columbia, Missouri, USA[a]; Department of Molecular Microbiology and Immunology, University of Missouri School of Medicine, Columbia, Missouri, USA[b]; Center for Drug Design, University of Minnesota, Minneapolis, Minnesota, USA[c]; Department of Microbiology and Molecular Genetics, University of Pittsburgh School of Medicine, Pittsburgh, Pennsylvania, USA[d]; and Department of Biochemistry, University of Missouri, Columbia, Missouri, USA[e]

RNase H inhibitors (RNHIs) have gained attention as potential HIV-1 therapeutics. Although several RNHIs have been studied in the context of HIV-1 reverse transcriptase (RT) RNase H, there is no information on inhibitors that might affect the RNase H activity of other RTs. We performed biochemical, virological, crystallographic, and molecular modeling studies to compare the RNase H function and inhibition profiles of the gammaretroviral xenotropic murine leukemia virus-related virus (XMRV) and Moloney murine leukemia virus (MoMLV) RTs to those of HIV-1 RT. The RNase H activity of XMRV RT is significantly lower than that of HIV-1 RT and comparable to that of MoMLV RT. XMRV and MoMLV, but not HIV-1 RT, had optimal RNase H activities in the presence of Mn^{2+} and not Mg^{2+}. Using hydroxyl-radical footprinting assays, we demonstrated that the distance between the polymerase and RNase H domains in the MoMLV and XMRV RTs is longer than that in the HIV-1 RT by ~3.4 Å. We identified one naphthyridinone and one hydroxyisoquinolinedione as potent inhibitors of HIV-1 and XMRV RT RNases H with 50% inhibitory concentrations ranging from ~0.8 to 0.02 μM. Two acylhydrazones effective against HIV-1 RT RNase H were less potent against the XMRV enzyme. We also solved the crystal structure of an XMRV RNase H fragment at high resolution (1.5 Å) and determined the molecular details of the XMRV RNase H active site, thus providing a framework that would be useful for the design of antivirals that target RNase H.

HIV-1 reverse transcriptase (RT) is vital for viral replication and has been a key target of antiviral therapies. The enzyme has three activities: RNA-dependent DNA polymerase activity to synthesize a cDNA strand using the positive-strand RNA viral genome as a template, RNase H activity to remove the viral RNA template during cDNA synthesis, and DNA-dependent DNA polymerase activity to complete the synthesis of the double-stranded DNA (dsDNA) using the cDNA as a template (50). While most approved anti-HIV drugs target RT, all of the approved RT drugs inhibit only the polymerase activity of the enzyme. Eventually, patients on antiretroviral therapy develop resistance to these drugs (3, 49, 68, 73), rendering them ineffective. Because of this, there are extensive efforts to identify new targets for the development of HIV therapeutics.

One such target is the RNase H activity of HIV-1 RT, which is the only enzymatic activity of the virus that has yet to be addressed by antiretroviral drugs. Such drugs would likely be active against all current drug-resistant viral strains, because the RNase H active site is located at the opposite end of the enzyme from the polymerase domain (~50 Å away) that is currently targeted by nucleoside and nonnucleoside RT inhibitors (79). Several compounds have been found in recent years to effectively inhibit the RNase H activity of HIV-1 RT, including α,γ-diketo acids and derivatives (27, 77, 78, 91), pyrimidinol carboxylic acids (43, 47), hydroxytropolones (including β-thujaplicinol) (6, 12, 15, 21, 34), dimeric lactones (19), 1,3,4,5-tetragalloylapiitol (86), phenolic glycosides (10), vinylogous ureas (16, 94), *N*-hydroxyimides (33, 44), 2-hydroxyisoquinoline-1,3(2*H*,4*H*)-diones (8, 9), acylhydrazones (11, 30, 35, 80), and naphthyridinones (84, 95). Although these inhibitors have been studied for the ability to inhibit HIV-1 RT, little is known about their effectiveness against other retroviral RTs, such as the gammaretroviral Moloney murine leukemia virus (MoMLV) and xenotropic murine leukemia virus-related virus (XMRV) RTs.

HIV-1 RT is structurally very different from the gammaretroviral MoMLV RT, which is closely related to XMRV RT in sequence and presumably in structure (17, 28, 29, 61). HIV-1 RT exists as a heterodimer composed of two subunits: an enzymatically active 66-kDa p66 domain, which contains the polymerase domain (composed of the fingers, palm, thumb, and connection subdomains) and the RNase H domain, and a 51-kDa p51 domain, which mainly provides structural support and has an amino acid sequence identical to that of p66 but does not contain the RNase H domain, which is removed by proteolytic cleavage (38, 45, 72, 75, 79). MoMLV RT is a 74-kDa monomer in the published crystal structures (17, 18, 29, 60), lacking the structural support

Received 26 October 2011 Returned for modification 16 November 2011
Accepted 5 January 2012
Published ahead of print 17 January 2012
Address correspondence to Stefan G. Sarafianos, sarafianoss@missouri.edu.
K.A.K. and B.M. contributed equally to this report.

doi:10.1128/AAC.06000-11

that p51 provides for HIV-1 RT. MoMLV RT may make up for this lack of structural support by possibly forming a homodimer during DNA synthesis (90). Although MoMLV and XMRV RTs share a strikingly high sequence identity (95%), most of the differences lie in the RNase H domain (61). Thus, studies of the RNase H function, structure, and inhibition of these enzymes should provide insights into the differences between the gammaretroviral and lentiviral enzymes and aid the design of novel, potent inhibitors of retroviral RNase H activity.

Here we used biochemical methods to determine the differences in RNase H activity caused by acylhydrazone-, naphthyridinone-, and hydroxyisoquinolinedione-based RNase H inhibitors (RNHIs) and compare their effectiveness against XMRV RT with their effectiveness against HIV-1 RT. The crystal structure of the isolated XMRV RNase H domain also provides a structural basis for the function and inhibition of gammaretroviral RNase H activity.

MATERIALS AND METHODS

Compounds. Naphthyridinone {4-[(4′-aminomethyl-1,1′-biphenyl)methyl]-1-hydroxy-1,8-naphthyridin-2-one (NAPHRHI)} and acylhydrazone (trihydroxy benzoyl naphthyl hydrazone [THBNH] and trihydroxy benzoyl biphenyl carboxylate hydrazone [BHMP07]) RNHIs were synthesized as previously reported (23, 30, 35, 95; U.S. patent application 20100056516). The hydroxyisoquinolinedione RNHI 7-(furan-2-yl)-2-hydroxy-isoquinoline-1,3(2*H*,4*H*)-dione (YLC2-155) was synthesized in Zhengqiang Wang's laboratory (University of Minnesota, Minneapolis, MN). The hydroxyisoquinolinedione compound was originally designed to inhibit hepatitis C virus NS5B polymerase (13).

Plasmid construction. Plasmid pBSK-XMRV, containing the coding sequence of XMRV RT from the VP62 clone (GenBank accession no. DQ399707.1), was synthesized and optimized for *Escherichia coli* expression by Epoch Biolabs Inc. The 2,013-bp XMRV RT sequence was amplified from pBSK-XMRV by PCR, with NdeI and HindIII restriction sites (61), and cloned into a pET28a vector. Construct pET-28a-MRT, encoding full-length (FL) wild-type MoMLV RT, was provided by Mukund Modak (New Jersey Medical School, Newark, NJ). HIV-1 RT was cloned into a pETDuet-1 vector and purified as previously described (4, 32, 56, 75). Plasmid pCSR231, encoding protein p15-Ec, a catalytically active chimeric HIV-1 RNase H domain fragment containing an α-helical substrate binding loop derived from *E. coli* RNase H1 (41, 78, 83), was a generous gift from Daria Hazuda (Merck, West Point, PA).

A DNA amplicon coding for amino acids 498 to 671 of XMRV RT was ligated into the bacterial expression vector pGEX-4T-1 (GE Healthcare Life Sciences) using restriction enzymes BamHI and XhoI. The resulting construct allows for the expression of a glutathione *S*-transferase (GST)-RNase H fusion protein that is cleavable with thrombin. A second XMRV RNase H construct was generated as described above with a deletion of residues 595 to 605 (helix C), resulting in a GST-RNase H ΔC fusion protein.

Protein expression and purification. Expression and purification of MoMLV and XMRV RTs were carried out similarly to previously published protocols (14, 40, 61). HIV-1 RNase H domain p15-Ec was expressed and purified as described previously (30).

The FL XMRV RNase H domain and the XMRV RNase H domain without helix C (residues 595 to 605; ΔC RNase H) were expressed in *E. coli* BL-21 as previously described for MoMLV RNase H (51). The FL and ΔC RNase H proteins were purified by GST column chromatography, followed by overnight cleavage of the GST tag with thrombin, and further purified by size exclusion chromatography as previously described (56).

RNase H activity assays. A 5′-Cy3-labeled RNA template (5′-Cy3-GGAAAUCUCUAGCAGUGGCGCCCGAACAGGGACCU) was heat annealed to a 3-fold molar excess of DNA primer (5′-AGGTCCCTGTTC GGGCGCCACT) to yield a Cy3-T_{r35}/P_{d22} RNA-DNA substrate as previously described (24). HIV-1 RT (20 nM) was incubated with RNA-DNA duplex (50 nM) at 37°C in buffer containing 50 mM Tris (pH 7.8), 60 mM KCl, 0.1 mg/ml bovine serum albumin (BSA), 0.01% NP-40, 2 mM dithiothreitol (DTT), and 0.5 mM EDTA. RNase H assays of MoMLV RT and XMRV RT were performed using 20 nM and 100 nM enzymes, respectively. Reactions were initiated by the addition of 6 mM $MgCl_2$ (for HIV-1 RT) or 0.5 mM $MnCl_2$ (for XMRV and MoMLV RTs). Aliquots of the reactions were stopped at the indicated time points by adding an equal volume of 100% formamide containing bromophenol blue. RNase H cleavage products were resolved on 15% polyacrylamide–7 M urea gels, which were scanned using a PhosphorImager (FujiFilm FLA 5000). Bands of uncleaved RNA-DNA duplex were quantified using Multi Gauge (FujiFilm). Values of calculated percent RNA-DNA duplex were plotted as a function of time using GraphPad Prism 4 (GraphPad Software, Inc.) to determine the rate of cleavage, k (min^{-1}), using the one-phase exponential-decay equation $Y = Y_0(e^{-kt}) + C$, where Y is % RNA-DNA duplex, Y_0 is the difference in activity maxima and minima, and e^{-kt} is the exponential decay with rate k relative to time t.

Site-specific hydroxyl-radical footprinting assay. 5′-Cy3-T_{d43}/P_{d30} (50 nM) was incubated with HIV-1 RT (600 nM) or XMRV RT (1 μM) in 120 mM sodium cacodylate (pH 7)–20 mM NaCl–5 mM $MgCl_2$–5 μM ddATP to allow quantitative chain termination. Prior to treatment with Fe^{2+}, complexes were preincubated for 7 min with the next nucleotide (dTTP; 500 μM) or phosphonoformic acid (PFA; 0 to 100 μM). The complexes were treated with 1 mM ammonium iron sulfate as previously described (53). This reaction relies on Fe^{2+} autoxidation (7) to create a local concentration of hydroxyl radicals, which cleave DNA at the nucleotide closest to the Fe^{2+} specifically bound to the RNase H active site. The ternary complexes with dTTP and PFA indicated the relative positions of the RNase H site with respect to the 3′ primer terminus under post- and pretranslocation conditions, respectively (69, 70, 93).

RNase H inhibition assays. We used the following RNase H substrates: HTS-1 (5′-GAUCUGAGCCUGGGAGCU-fluorescein-3′ annealed to 5′-Dabcyl-AGCTCCCAGGCTCAGATC-3′), which induces random or nonspecific RNA cleavage, and HTS-2 (5′-CUGGUUAGACC AGAUCUGAGCCUGGGAGCU-fluorescein-3′ annealed to 5′-Dabcyl-A GCTCCCAGGCTCAGATC-3′), which induces 3′-mediated RNA cleavage. When the RNA and DNA strands of each substrate are annealed together, the fluorescence signal of the fluorescein is quenched by the Dabcyl. After RNA cleavage, the fluorescein-labeled RNA fragment dissociates from the DNA strand, resulting in a measurable fluorescence signal. Susceptibility assays using RNHIs were performed as previously described, with some modifications (65). The HIV-1 RT RNase H reaction buffer contained 50 mM Tris (pH 7.8) and 50 mM NaCl, while the XMRV reaction buffer contained 50 mM Tris (pH 7.8), 60 mM KCl, 0.1 mg/ml BSA, 0.01% NP-40, and 1 mM DTT. Dilutions of RNHIs were prepared using 100% dimethyl sulfoxide (DMSO) so that the final concentration in the reaction was 1%. Random-cleavage assay mixtures included 100 nM HTS-1, 20 nM enzyme, and 5 mM $MgCl_2$ (HIV-1 RT) or 0.5 mM $MnCl_2$ (XMRV RT), and various concentrations of inhibitors were incubated for 20 min at 37°C. 3′-mediated cleavage was assessed in reaction mixtures containing 100 nM HTS-2. Reactions were quenched by the addition of EDTA to a final concentration of 33 mM. Fluorescence signals were measured using an excitation wavelength of 485 nm and an emission wavelength of 528 nm in an EnSpire Multimode Plate Reader (Perkin-Elmer). The results from dose-response experiments were plotted using GraphPad Prism 4, and 50% inhibitory concentrations (IC_{50}s) were obtained at midpoint concentrations (22). Reactions were performed in duplicate.

Susceptibility assays using RNase H fragments (XMRV FL RNase H or p15-Ec) to RNHIs were performed similarly to the procedure described for the RTs. A 200 nM concentration of FL RNase H or a 20 nM concentration of p15-Ec was incubated with 250 nM HTS-1 or HTS-2 in the presence of 0.5 mM $MnCl_2$ for 20 min at 37°C. Reactions were performed in duplicate. IC_{50}s were determined as described above.

Polymerase inhibition assays. Template DNA (5′-ATGTGTGTGC CCGTCTGTTGTGTGACTCTGGTAACTAGAGATCCCTCAGACCCT

TTTAGTCAGTGTGGAATATCTCATAGCTTGGCGCCCGAACAGG GAC) was heat annealed in an equimolar amount to a DNA primer (5′-GTCCCTGTTCGGGCGCCA) to yield a T_{d100}/P_{d18} DNA-DNA substrate as previously described (56). The polymerase reaction buffer contained 50 mM Tris (pH 7.8) and 50 mM NaCl. Dilutions of compounds were prepared using 100% DMSO so that the final concentration in the reaction was 1%. For HIV-1 RT, 0.5 mM EDTA, 50 nM T_{d100}/P_{d18}, 1 μM deoxynucleotide triphosphates (dNTPs), and 20 nM HIV-1 RT were incubated in the reaction buffer before initiation of the reaction with 6 mM $MgCl_2$ and various concentrations of inhibitors. For XMRV RT, 0.05 mM EDTA, 40 nM T_{d100}/P_{d18}, 50 μM dNTPs, and 100 nM XMRV RT were incubated in the reaction buffer before initiation of the reaction with 0.6 mM $MnCl_2$ and various concentrations of inhibitors. Reactions were run at room temperature for 30 min, quenched by the addition of 50 μl of 100 mM EDTA and 2× Quant-iT PicoGreen dsDNA reagent (Invitrogen) to quantify the amount of dsDNA present in solution. Fluorescence signals were measured using an excitation wavelength of 480 nm and an emission wavelength of 520 nm in an EnSpire Multimode Plate Reader. To assess the effects of the inhibitors, the fluorescence signal was plotted using GraphPad Prism 4 to determine the IC_{50}s.

Cell-based inhibitor susceptibility assays using pseudotyped and infectious viruses. Monolayer cultures of 293FT cells were seeded at 1×10^5/well in six-well plates. Six hours later, the cells were transfected with 350 ng of pGFP reporter-LTR, 300 ng of pVSV Env (vesicular stomatitis virus [VSV]), and 350 ng of pCMV-XMRV-Gag/Pol or pCMV-MoMLV-Gag/Pol to obtain XMRV or MoMLV pseudotyped with VSV Env (61). To prepare HIV-1 pseudotyped with VSV Env, we used the above-described transfection protocol but with 500 ng of pCMV-HIV-GFP and 500 ng of pVSV Env. Culture supernatants from 293FT cells were collected 48 h after transfection, clarified by centrifugation at 1,100 rpm in a swinging-bucket rotor for 5 min, and filtered through 0.45-μm-pore-size sterile filters. Virus-containing supernatants were serially diluted and used to infect target cells at various inhibitor concentrations. Azidothymidine (AZT) and 4′-ethynyl-2-fluoro-2′-deoxyadenosine (EFdA) were used as controls (56, 64). Target cells for pseudotype assays were MAGIC-5 cells. At 48 h postinfection, the green fluorescent protein (GFP)-expressing cells were counted under a fluorescence microscope. Drug concentrations reducing the number of infected cells to 50% of the drug-free control (50% effective concentrations [EC_{50}s]) were determined from dose-response curves.

For fully infectious virus, we used HIV-1 laboratory strain NL4-3, which was obtained from the AIDS Research and Reference Reagent Program at the National Institutes of Health (NIH). 293T cells were transfected with pNL4-3 by FuGENE 6 (Roche). Supernatants containing NL4-3 were harvested 72 h after transfection and stored at −80°C until use. Susceptibility to EFdA and NAPHRHI was determined using MAGIC-5 cells (CCR5-expressing HeLa/$CD4^+$ cell clone) (31). Briefly, MAGIC-5 cells were infected with a diluted virus stock (100 blue forming units) in the presence of increasing concentrations of RNHI. Forty-eight hours after viral exposure, the blue cells stained with X-Gal (5-bromo-4-chloro-3-indolyl-β-D-galactopyranoside) were counted under a light microscope. Susceptibility to AZT and YLC2-155 was determined using TZM cells as previously described (58), while susceptibility to BHMP07 and THBNH was determined using CEM cells (36). EC_{50}s were determined from dose-response curves as described for pseudotype-based assays and previously (61).

Cytotoxicity assay. Cytotoxic effects of the various compounds were evaluated using an XTT cell viability kit (Biotium Inc.). XTT [2,3-bis-(2-methoxy-4-nitro-5-sulfophenyl)-2H-tetrazolium-5-carboxanilide] is a tetrazolium derivative. This assay measures cell viability based on the activity of mitochondrial enzymes in live cells that reduce the XTT reagent and are inactivated shortly after cell death. The amount of product generated from XTT is proportional to the number of living cells in the sample and can be quantified by measuring absorbance at a wavelength of 475 nm. Briefly, the compounds were tested in triplicate experiments in a 96-well plate format. Ten thousand cells per well (100 μl) were incubated at 37°C with various amounts of the compounds. After 48 h, 25 μl of the XTT reagent was added to each well and incubated for 3 h before absorbance measurement at a wavelength of 475 nm and a reference wavelength of 660 nm. As the compound concentration increases, the absorption decreases. Percent absorption values of the compounds were determined relative to that of a control that did not contain inhibitor and plotted in GraphPad Prism 4 to obtain 50% cytotoxic concentrations (CC_{50}s).

Crystallization and data collection. XMRV ΔC RNase H was concentrated to 22 mg/ml and used with several crystal screening kits (Hampton Research and Qiagen) by sitting-drop vapor diffusion at 18°C. Hits from the initial screening conditions were optimized into large bundles of needles grown in 27% polyethylene glycol (PEG) 1500 and 0.1 M sodium citrate, pH 4.7. Thin needles were observed within 24 h, and the crystals grew larger after 3 to 4 days. Crystals were typically soaked in a solution containing 5 mM $MgCl_2$ and RNHI for 2 h.

XMRV RNase H ΔC crystals soaked with $MgCl_2$ and inhibitor were cryoprotected with reservoir solution containing 17% PEG 200. Single needles diffracted to high resolution at Beamline 4.2.2 of the Advanced Light Source at Lawrence Berkeley National Laboratory. The data were processed using d*TREK (67). The ΔC RNase H crystals were of space group $P4_1$ and had unit cell dimensions of $a = 37.5$ Å and $c = 100.7$ Å. One monomer was present in the asymmetric unit, and the Matthews coefficient was 2.1 $Å^3$/Da, corresponding to a solvent content of 40.6% (54).

Phase determination and structure refinement. The structure was determined by molecular replacement using Phaser (55). The crystal structure of the MoMLV RNase H domain (Protein Data Bank [PDB] code 2HB5) was used as a search model. After initial rigid-body, TLS, and restrained refinement in Phenix (1), R_{work} dropped to 0.299 with an R_{free} of 0.316. A simulated annealing protocol was also run during refinement to remove model bias. An initial model was built using ARP/wARP (46, 66) with refinement using Refmac (57, 59). Several cycles of model building and refinement were carried out using Coot (25) and Phenix, respectively. The final model was validated using MolProbity (20). Final refinement statistics are listed in Table 1.

Molecular modeling. To obtain a model of the XMRV ΔC RNase H bound to nucleic acid, the XMRV ΔC RNase H structure was superposed onto a structure of HIV-1 RT in complex with an RNA-DNA substrate (PDB ID, 1HYS) (71) using the PyMOL molecular graphics software (74). Minor adjustments to side chain positions were made to relieve any steric interactions in Coot.

Protein structure accession number. The atomic coordinates and structure factors determined in this study have been deposited in the Research Collaboratory for Structural Bioinformatics PDB and are available under accession code 3P1G.

RESULTS

Dependence of RNase H activity on divalent metal. In order to compare the RNase H activities of XMRV, MoMLV, and HIV-1 RTs, we performed time-dependent RNase H activity assays in the presence of Mg^{2+} and Mn^{2+}. The RNase H cleavage patterns of the Cy3-T_{r35}/P_{d22} RNA-DNA by HIV-1, MoMLV, and XMRV RTs were different. HIV-1 RNase H showed a primary cut at approximately18 bp upstream from the 3′ primer end, whereas both the MoMLV and XMRV RNases H showed a primary cut at approximately 19 bp from the 3′ primer end (Fig. 1A), suggesting a difference in the distance between the polymerase and RNase H active sites. HIV-1 RNase H activity is slightly faster in the presence of Mg^{2+} than Mn^{2+} (rates of RNA-DNA cleavage [k] were 3.0 and 1.9 min^{-1}, respectively), while XMRV and MoMLV RNase H showed 4- to 6-fold increased rates of cleavage (k) in the presence of Mn^{2+} versus Mg^{2+} (Fig. 1B). Similarly, we have recently reported that the polymerase activities of both the MoMLV and XMRV RTs are higher in the presence of Mn^{2+} (61). We also

TABLE 1 X-ray data collection and refinement statistics

Parameter	Value
Wavelength (Å)	1.0
Resolution (Å)	1.50 (1.55–1.50)[a]
Space group	$P4_1$
Cell dimensions	
a, *c* (Å)	37.5, 100.7
No. of observed reflections	150,720
No. of unique reflections	22,272
Redundancy	6.8 (3.7)
Completeness (%)	99.9 (99.3)
R_{sym}[b]	0.098 (0.771)
Avg I/σ ratio	7.8 (2.1)
Refinement statistics	
Resolution (Å)	37.53–1.50
No. of reflections	
Working	21,970
Test	1,122
R_{work}[c]	0.161
R_{free}[d]	0.182
No. of water molecules	162
Overall B value (Å^2)	28.24
Wilson B value (Å^2)	20.23
RMSD bond length (Å)	0.006
RMSD angle (°)	0.995
Ramachandran plot (%)[e]	
Favored	98.4
Allowed	1.6
Disallowed	0.0

[a] Values in parentheses are for the highest-resolution shell.
[b] $R_{sym} = \Sigma_{hkl} |I - <I>|/\Sigma_{hkl} |I|$.
[c] $R_{work} = \Sigma_{hkl} |F_{obs} - F_{calc}|/\Sigma_{hkl} |F_{obs}|$.
[d] $R_{free} = R_{cryst}$, except 5% of the data were excluded from the refinement.
[e] Evaluated by MolProbity (20).

tested both the FL and ΔC constructs of the isolated XMRV RNase H domain for RNase H activity. We found that the FL XMRV RNase H had considerable RNase H activity, although it was lower than that of the XMRV RT enzyme. We also found that the XMRV ΔC RNase H also demonstrated RNase H activity comparable to that of the FL XMRV RNase H domain.

Relative distance between the polymerase and RNase H sites of RTs. To confirm the potential difference in the distance between the polymerase and RNase H active sites suggested from the RNase H cleavage experiments, we used a hydroxyl-radical footprinting assay that precisely determines the position of the RNase H cleavage with respect to the polymerase active site (Fig. 2). As expected for both enzymes, addition of increasing amounts of the incoming dNTP results in the formation of more RT-DNA complex in a posttranslocation state, whereas addition of PFA favors binding of RT in a pretranslocation state. Notably, at this specific site, in the absence of either dTTP or PFA, most of the enzyme is at a posttranslocation state (−17 for HIV-1 RT and −18 for XMRV RT). Hence, for the HIV-1 and XMRV RTs, the pretranslocation states (in the presence of PFA) are 18 and 19 bp upstream from the primer's 3′ end (Fig. 2).

Inhibition of RNase H activity. To compare the susceptibilities of the XMRV and HIV-1 RTs to RNHIs, we performed a fluorescence-based assay (65). Two different RNA-DNA substrates were used: HTS-1, a blunt-ended, polymerase-independent substrate that induces nonspecific RNA cleavage, and HTS-2, a polymerase-dependent substrate that induces 3′-mediated RNA cleavage. The BHMP07 acylhydrazone and NAPHRHI naphthyridinone compounds have been previously shown to inhibit HIV-1 RT RNase H (30, 95). The acylhydrazone THBNH is similar to the previously reported dihydroxy benzoyl naphthyl hydrazone (35). While some hydroxyisoquinolinediones are known RNHIs (8, 9), YLC2-155 has not been tested against RNase H. Our results showed that two of the four inhibitors (NAPHRHI and YLC2-155) effectively inhibited nonspecific RNA cleavage by both HIV-1 and XMRV RTs (Fig. 3B). BHMP07 and THBNH were both potent inhibitors of random RNA cleavage by HIV-1 RT (IC_{50}s, 96 and 177 nM) but less effective against XMRV RT (IC_{50}s, 1,305 and 1,446 nM). NAPHRHI was the most potent inhibitor of nonspecific RNA cleavage by both the HIV-1 and XMRV RTs (IC_{50}s, 21 and 8 nM). Random RNA cleavage by XMRV RNase H domain was also sensitive to NAPHRHI (IC_{50}, 357 nM), but not the acylhydrazone or hydroxyisoquinolinedione inhibitors. Interestingly, XMRV ΔC RNase H was not inhibited by NAPHRHI. All four compounds tested were highly effective against nonspecific RNA cleavage by the p15-Ec HIV RNase H fragment, with IC_{50}s ranging from 18 to 56 nM. YLC2-155 was more potent against XMRV than HIV-1 RT. Although this compound was highly effective against XMRV RT, it was less effective against the XMRV RNase H domain.

Similar to the inhibition of nonspecific RNA cleavage, NAPHRHI and YLC2-155 were also potent inhibitors of 3′-mediated RNA cleavage by both the HIV-1 and XMRV RTs (Fig. 3C). BHMP07 and THBNH were both effective inhibitors of 3′-mediated RNA cleavage by HIV-1 RT (IC_{50}s, 287 and 552 nM) but less effective against XMRV RT (IC_{50}s, 851 and 1,609 nM). Overall, the compounds more efficiently inhibited nonspecific, rather than 3′-mediated, RNA cleavage by HIV-1 RT. 3′-mediated cleavage by XMRV RNase H was also inhibited by NAPHRHI (IC_{50}, 402 nM) but not by the other compounds. This result confirms that NAPHRHI efficiently inhibits XMRV RT RNase H activity. Similar to the results observed for nonspecific RNA cleavage, all four RNHIs were also potent inhibitors of 3′-mediated cleavage by the p15-Ec HIV RNase H fragment.

In order to better understand the mechanism of action of the most potent inhibitor of XMRV RT, NAPHRHI, we tested the effect of varying the NAPHRHI and RNA-DNA preincubation conditions on the inhibition of the RNase H activities of the HIV-1 and XMRV RTs and of XMRV RNase H (Fig. 4). We tested the following combinations of preincubation conditions of the four reaction components: enzyme plus NAPHRHI, enzyme plus NAPHRHI plus $MgCl_2$ or $MnCl_2$, enzyme plus NAPHRHI plus RNA-DNA substrate (HTS-1), and enzyme plus HTS-1. After incubation at 37°C for 5 min, the reactions were initiated by addition of the missing components. The results reveal that the preincubation conditions do not significantly affect the ability of NAPHRHI to inhibit the RNase H activity of HIV-1 RT in the presence of Mg^{2+} (Fig. 4A) or XMRV RT in the presence of Mn^{2+} (Fig. 4C). However, preincubation of XMRV RNase H with RNA-

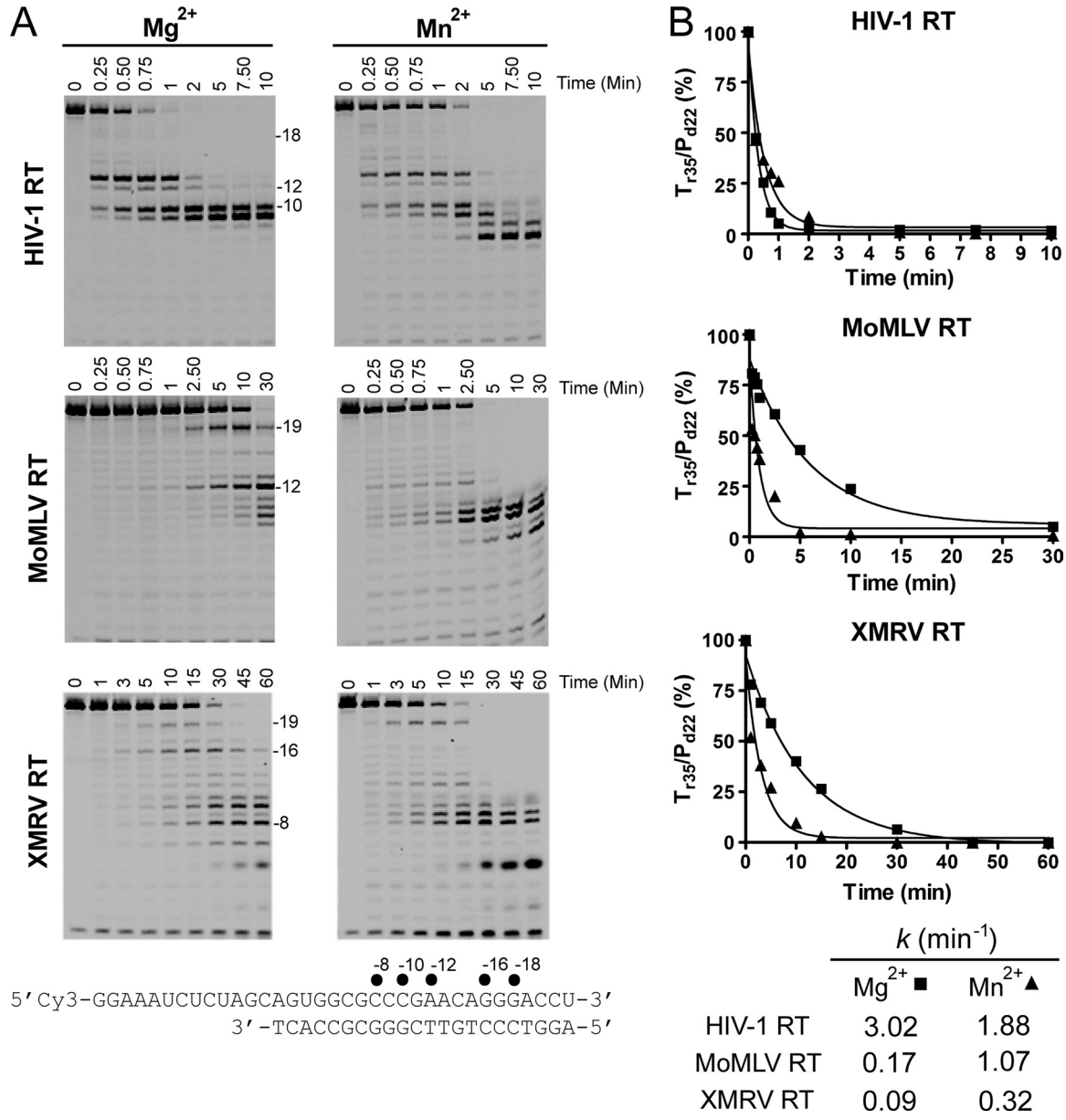

FIG 1 Dependence of RNase H activity on metal and time for HIV-1, MoMLV, and XMRV RTs. (A) A 50 nM concentration of Cy3-T_{r35}/P_{d22} was incubated with 20 nM HIV-1 RT or MoMLV RT or 100 nM XMRV RT for the indicated times. Lengths of cleavage products are indicated. (B) Quantification of cleavage products shown in panel A. Percent RNA-DNA duplex was plotted as a function of time to determine the rate of cleavage, k (min^{-1}), by each enzyme.

DNA in the presence of Mn^{2+} appeared to decrease the ability of NAPHRHI to inhibit the RNase H fragment (Fig. 4E).

To confirm that the presence of nucleic acid does not compete with the binding of NAPHRHI, we tested the effect of the RNA-DNA concentration on the potency of XMRV RNase H inhibition by NAPHRHI side by side with another RNHI, β-thujaplicinol, which is known to lose its inhibitory effect when the target enzyme is preincubated with the RNA-DNA substrate (Table 2) (6). The reaction mixtures were preincubated with XMRV RNase H, $MnCl_2$, and various concentrations of NAPHRHI or β-thujaplicinol before initiation of the reaction with different concentrations of HTS-1 RNA-DNA. As the RNA-DNA concentration was increased, NAPHRHI remained a potent inhibitor of XMRV RNase H (IC_{50}s between 190 and 414 nM). β-Thujaplicinol was able to inhibit XMRV RNase H in the presence of 200 nM HTS-1 RNA-DNA substrate (IC_{50}, 1.4 μM). However, as expected, β-thujaplicinol was not able to inhibit XMRV RNase H as the concentration of RNA-DNA substrate was increased.

Inhibition of polymerase activity. In order to determine if the RNHIs also inhibit the polymerase activity of HIV-1 and XMRV RTs, we performed polymerase inhibition assays using the Quant-iT PicoGreen dsDNA reagent, which is an ultrasensitive fluorescent nucleic acid stain used to quantify the amount of dsDNA in solution. The results indicate that, in general, the compounds are less effective at inhibition of polymerase activity than RNase H activity, with IC_{50}s for polymerase activity between 1 and

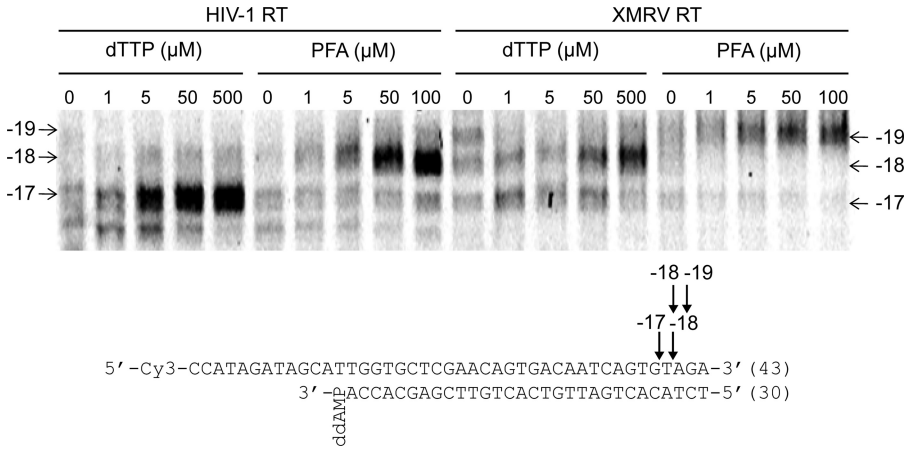

FIG 2 Use of site-specific Fe^{2+} footprinting assay to determine the translocation state of RTs bound to DNA. The translocation state of RTs was determined using hydroxyl radical footprinting. A 50 nM concentration of 5′-Cy3-$T_{d43}/P_{d30\text{-}ddA}$ chain terminated with ddA was incubated with HIV-1 RT (600 nM) or XMRV RT (1 μM) and a 0 to 500 μM concentration of the next incoming nucleotide (dTTP) to induce the formation of posttranslocation complexes or a 0 to 100 μM concentration of PFA to induce the formation of pretranslocation complexes. The complexes were treated for 5 min with ammonium iron sulfate (1 mM) and resolved on polyacrylamide–7 M urea gel. For HIV-1 RT, cleavages at positions −18 and −17 from the 3′-OH of the primer strand indicate pre- and posttranslocation complexes, respectively. In the case of XMRV RT, the corresponding complexes are at positions −18 and −19, suggesting a slightly longer distance between the polymerase and RNase H active sites.

100 μM. The naphthyridinone NAPHRHI was the most effective RNHI against the polymerase activity of both the HIV-1 and XMRV RTs (IC_{50}, 5 μM for both enzymes). Acylhydrazones BHMP07 and THBNH and hydroxyisoquinolinedione YLC2-155 were able to inhibit the polymerization activity of HIV-1 RT in the low micromolar range (IC_{50}, 4 to 9 μM). On the other hand, only BHMP07 and THBNH were able to inhibit the polymerization activity of XMRV RT (IC_{50}s, 16.5 and 31.6 μM, respectively). These results reveal that the most potent RNHIs (naphthyridinone NAPHRHI and hydroxyisoquinolinedione YLC2-155) demonstrate selectivity for inhibition of the RNase H activity of HIV-1 and XMRV RTs over inhibition of the polymerase activity of these enzymes.

Antiviral properties of RNHIs in cell-based assays. To determine the susceptibility of retroviruses to RNHIs *in vivo*, we performed single-cycle viral replication assays using XMRV, MoMLV, and HIV-1 with the gene for GFP as a reporter. The viruses were pseudotyped with VSV envelope (VSV-G) (Table 3). We used AZT as a positive control of viral inhibition and confirmed previous reports that, similar to HIV-1, XMRV and MoMLV are highly susceptible to AZT (64). We also showed that XMRV and MoMLV are also susceptible to EFdA, with an EC_{50} higher than that for HIV-1 (by 78- and 70-fold, respectively). The naphthyridinone RNHI NAPHRHI inhibited XMRV or MoMLV by ~30% at a concentration of 2 μM. However, it was not possible to reliably assess its antiviral potency because NAPHRHI showed signs of cytotoxicity at a concentration of 4.1 μM. NAPHRHI was slightly more active against pseudotyped HIV by blocking 50% of infection at 1.3 μM.

We also tested the RNHIs in cell-based assays using fully infectious HIV-1 (strain NL4-3, Table 4). AZT and EFdA were used as controls. The acylhydrazone compounds BHMP07 and THBNH demonstrated inhibition of infectious HIV at EC_{50}s of 2.5 and 3.0 μM, respectively. The hydroxyisoquinolinedione compound YLC2-155 was slightly less efficient, with an EC_{50} of 6.7 μM. However, the naphthyridinone compound NAPHRHI was able to potently inhibit infectious HIV-1 NL4-3 (EC_{50} = 250 nM). NAPHRHI was also able to effectively inhibit HIV-1 MN with an EC_{50} of 180 nM, making NAPHRHI more effective at inhibition of the fully infectious virus than of the pseudotyped HIV.

Cytotoxicity of RNHIs. We tested the cytotoxic effects of the RNHIs with an XTT cell viability assay to assess their potential as therapeutics. This assay measures cell viability based on the activity of mitochondrial enzymes in live cells that reduce the XTT reagent and are inactivated shortly after cell death. The amount of product generated from XTT is proportional to the number of living cells in the sample and can be quantified by measuring absorbance at a wavelength of 475 nm. We found that CC_{50}s were greater than 100 μM for the acylhydrazone (BHMP07 and THBNH) and hydroxyisoquinolinedione (YLC2-155) compounds (Table 4). However, the NAPHRHI compound was more cytotoxic, with a CC_{50} of 4.1 μM.

Structure of XMRV ΔC RNase H. To better understand how the structure of XMRV RNase H may affect its function and inhibition by RNHIs, we pursued crystallization of the isolated XMRV RNase H domain to determine its molecular architecture. Parallel crystallization of both the FL and ΔC XMRV RNase H constructs was undertaken in anticipation that similar problems would arise in crystallizing the FL construct as had been observed with the MoMLV FL RNase H (51). After initial screening and further optimization, thick needles of XMRV ΔC RNase H were grown and diffracted X-rays to 1.5 Å, resulting in a high-resolution electron density map (Fig. 5A). Although these crystals were soaked with NAPHRHI inhibitor in the presence of $MgCl_2$, no inhibitor was observed in the electron density at the active site.

The structure of XMRV ΔC RNase H is similar to that of MoMLV ΔC RNase H, with some small differences. Like that of the MoMLV ΔC RNase H, the core of the XMRV ΔC RNase H structure contains a mixed β-sheet composed of five strands (four parallel and one antiparallel), flanked by four α-helices (Fig. 5B). The primary difference between the MoMLV and XMRV ΔC RNases H is at the C terminus; the XMRV ΔC RNase H α-helix E

A

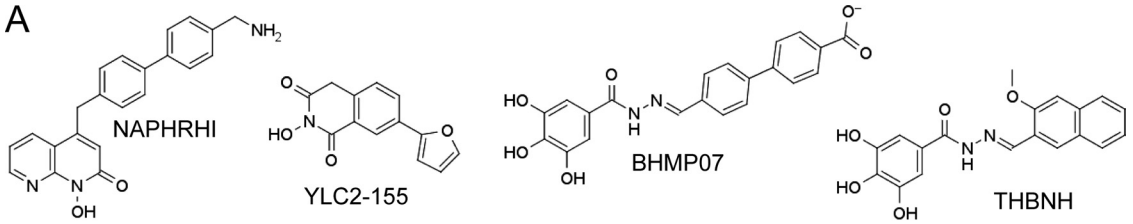

B

	IC_{50} (nM)			
	NAPHRHI	YLC2-155	BHMP07	THBNH
HIV-1 RT	20.6 ± 8.9	235 ± 56	95.5 ± 40.4	177 ± 114
p15-Ec HIV RNH	18.4 ± 0.2	52.8 ± 6.8	55.7 ± 11.7	31.3 ± 2.1
XMRV RT	7.7 ± 0.7	45.9 ± 5.9	1,305 ± 249	1,446 ± 168
XMRV RNH	357 ± 42	>10,000	>10,000	>10,000

HTS-1 (Polymerase Independent Substrate)

5′-GAUCUGAGCCUGGGAGCU-Fluorescein-3′
3′-CTAGACTCGGACCCTCGA-Dabcyl-5′

C

	IC_{50} (nM)			
	NAPHRHI	YLC2-155	BHMP07	THBNH
HIV-1 RT	104 ± 4	890 ± 94	287 ± 41	552 ± 112
p15-Ec HIV RNH	11.1 ± 3.7	371 ± 3	182 ± 10	225 ± 31
XMRV RT	6.2 ± 0.8	343 ± 128	851 ± 47	1,609 ± 445
XMRV RNH	402 ± 61	>10,000	>10,000	>10,000

HTS-2 (Polymerase Dependent Substrate)

5′-CUGGUUAGACCAGAUCUGAGCCUGGGAGCU-Fluorescein-3′
3′-CTAGACTCGGACCCTCGA-Dabcyl-5′

FIG 3 Inhibition of RNase H activity of HIV-1 and XMRV RTs and isolated XMRV and p15-Ec HIV RNases H by RNHIs. (A) RNHIs used in this study. (B) A 20 nM concentration of RT or p15-Ec HIV RNase H or 200 nM XMRV RNase H was preincubated with increasing concentrations of RNHIs at room temperature for 5 min. Reactions were initiated by the addition of 100 nM RNase H substrate HTS-1 for the RTs (250 nM HTS-1 for XMRV and p15-Ec HIV RNases H) in the presence of 5 mM $MgCl_2$ (HIV-1 RT) or 0.5 mM $MnCl_2$ (XMRV enzymes and p15-Ec). After 20 min of incubation at 37°C, reactions were quenched with EDTA. The results from dose-response experiments were plotted using GraphPad Prism 4, and IC_{50}s were obtained at midpoint concentrations. (C) Reactions were performed as described above, with minor variation. A 20 nM concentration of enzyme and 100 nM RNase H substrate HTS-2 were used for the RTs, while 20 nM p15-Ec HIV RNase H or 200 nM XMRV RNase H and 250 nM HTS-2 substrate was used for the RNase H assays. Reaction mixtures were incubated for 20 min at 37°C.

is longer than that of MoMLV ΔC RNase H. The differences between XMRV ΔC RNase H and HIV-1 RNase H are also similar to those found for MoMLV and HIV RNases H (51). XMRV ΔC RNase H has a longer β-sheet 1 and α-helix E and a shorter β-sheet 3 than HIV-1 RNase H. A sequence alignment of the RNase H domains of the XMRV, MoMLV, HIV-1, and *Bacillus halodurans* RTs shows the similarities among these enzymes, including the highly conserved active-site catalytic residues (Fig. 6). Because the MoMLV and XMRV RTs are highly homologous (95% sequence identity), the root mean square deviation (RMSD) of the MoMLV and XMRV RNH domains is 0.34 Å. Since the XMRV and HIV-1 RTs are less homologous (21% sequence identity), the RMSD of the XMRV and HIV-1 RNH domains is slightly higher at 1.6 Å.

Close inspection of the active site of XMRV ΔC RNase H showed one Mg^{2+} octahedrally coordinated to the three conserved acidic residues (Asp524, Glu562, and Asp583) that make up the catalytic core of the RNase H and two water molecules (Fig. 7A). This is similar to the active-site coordination observed in the MoMLV ΔC RNase H structure (51).

Model of XMRV ΔC RNase H bound to nucleic acid. In order to assess if the differences in structure between the XMRV ΔC and HIV-1 RNase H domains might have an effect on substrate binding, we modeled an RNA-DNA substrate with the XMRV ΔC RNase H structure. The XMRV ΔC RNase H domain was aligned with the RNase H domain of the HIV-1 RT-RNA-DNA complex (PDB ID, 1HYS) (71). Of the 568 amino acids that are different between the XMRV and HIV-1 RTs, 129 (23%) of them are in the RNase H domain. A total of seven residues of the XMRV ΔC RNase H domain appear to be at interacting distances from the RNA-DNA substrate: Arg534, Ser557, Gln559, and Lys612, which interact with the DNA primer strand, and Arg585, His638, and Arg657, which interact with the RNA template strand (Fig. 8A). Like HIV-1 RNase H, XMRV ΔC RNase H has a histidine which stabilizes the scissile phosphate in the proper position at the active site for cleavage (position 638 in XMRV, position 539 in HIV-1).

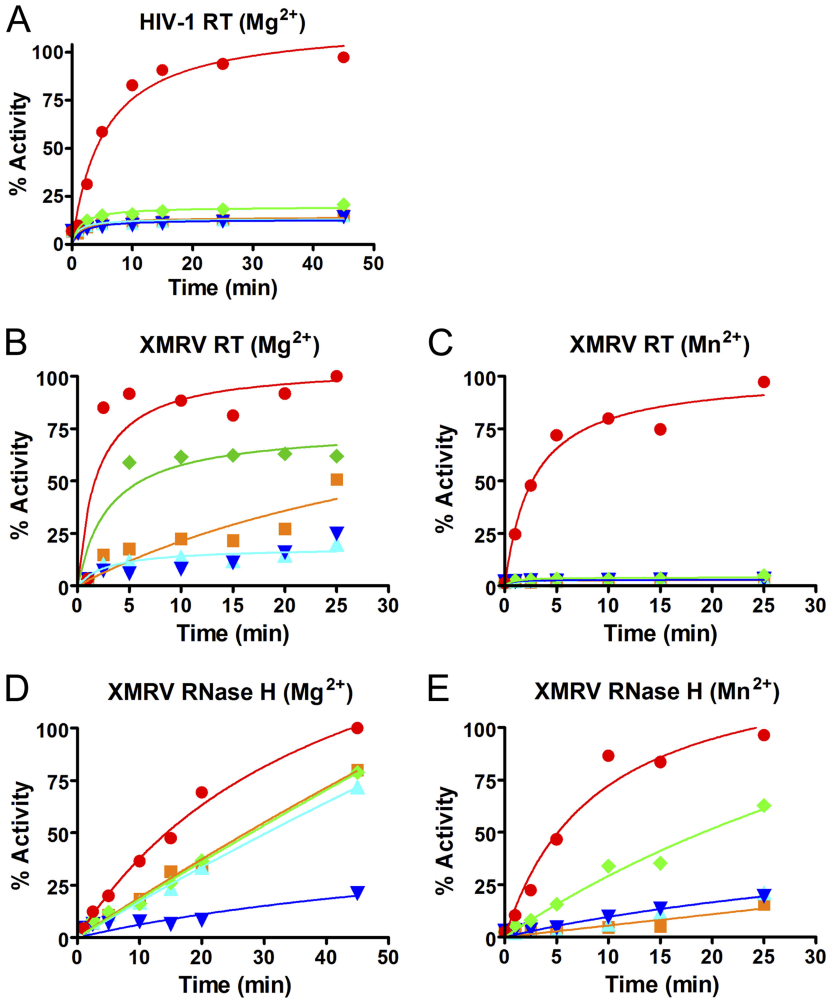

FIG 4 Effect of preincubation conditions on inhibition of RNase H. We used HIV-1 RT (A), XMRV RT in the presence of Mg^{2+} (B), XMRV RT in the presence of Mn^{2+} (C), XMRV RNase H in the presence of Mg^{2+} (D), and XMRV RNase H in the presence of Mn^{2+} (E). Each reaction mixture contained 20 nM RT or 200 nM RNase H, 500 nM NAPHRHI, 5 mM $MgCl_2$ or 0.5 mM $MnCl_2$, and 250 nM RNA-DNA (HTS-1) substrate. Assays were performed as described in Materials and Methods. The enzymes were preincubated with inhibitor (NAPHRHI), $MgCl_2$ or $MnCl_2$, and/or RNA-DNA (HTS-1) substrate under the following conditions at 37°C for 5 min prior to starting the reaction: ■, enzyme plus NAPHRHI; ▲, enzyme plus NAPHRHI plus $MgCl_2$ or $MnCl_2$; ▼, enzyme plus NAPHRHI plus HTS-1; ♦, enzyme plus HTS-1; ●, enzyme plus HTS-1 plus $MgCl_2$ or $MnCl_2$ (no-inhibitor control). The reactions were initiated by the addition of the missing components. The fluorescence signal was normalized to the highest fluorescence value of the uninhibited reaction to obtain percent activity.

Also helping to stabilize the RNA template in XMRV is Arg585, which interacts with the phosphate backbone of the RNA template 2 bases in front of (toward the 5′ end of the template) the scissile phosphate. In HIV-1 RNase H, there is a Gln500 at a similar position, but this residue interacts with the phosphate backbone of the RNA template only 1 base in front of the scissile phosphate (Fig. 8B). The last residue of the XMRV ΔC RNase H domain in contact with the RNA template is Arg657, which has a very weak interaction with the phosphate backbone of the RNA template 1 base behind (toward the 3′ end of the template) the scissile phos-

TABLE 2 Effect of RNA-DNA substrate concentration on potency of RNHIs[a]

Inhibitor	Mean IC_{50} (nM) ± SEM at [RNA-DNA] of:		
	200 nM	1,000 nM	5,000 nM
NAPHRHI	414 ± 153	283 ± 119	190 ± 107
β-Thujaplicinol	1,407 ± 714	>25,000	>25,000

[a] Reaction mixtures were preincubated with isolated XMRV RNase H (200 nM), $MnCl_2$ (0.5 mM), and various concentrations of NAPHRHI or β-thujaplicinol inhibitor before initiation of the reaction with different RNA-DNA (HTS-1) substrate concentrations. The experiments were done in triplicate.

TABLE 3 Susceptibilities of NRTIs and NAPHRHI to pseudotyped HIV-1, XMRV, and MoMLV

Inhibitor	Mean EC_{50} (μM) ± SEM		
	Pseudotyped HIV	Pseudotyped XMRV	Pseudotyped MoMLV
NRTIs			
AZT	0.0051 ± 0.0009	0.0081 ± 0.00005	0.0074 ± 0.0014
EFdA	0.0014 ± 0.0004	0.11 ± 0	0.098 ± 0.002
RNHI NAPHRHI	1.3 ± 0.2	>2[a]	>2[a]

[a] XMRV and MoMLV infectivities were 65 and 81%, respectively, in the presence of 2 μM NAPHRHI. Higher inhibitor concentrations resulted in cytotoxic effects.

TABLE 4 Susceptibilities of NRTIs and RNHIs to infectious HIV-1 NL4-3

Inhibitor	EC_{50} (μM)	CC_{50} (μM)	Selectivity index[a]
NRTIs			
AZT	0.180 ± 0.06	>100	>556
EFdA	0.0028 ± 0.0007	>100	>35,714
RNHIs			
NAPHRHI	0.250[b]	4.1 ± 0.2	16.4
YLC2-155	6.7 ± 0.8	>100	>14.9
BHMP07	2.5 ± 1.0	>100	>40
THBNH	3.0 ± 1.2	>100	>33

[a] Selectivity index = CC_{50}/EC_{50}.
[b] NAPHRHI was also tested against HIV-1 strain MN (EC_{50} = 180 nM).

phate. HIV-1 RNase H has additional residues that aid in stabilizing the RNA template: Asn474 and Gln475, which provide added stabilization near the scissile phosphate, and Arg448, which interacts in the minor groove of the nucleic acid with the RNA base containing the scissile phosphate (71). These additional interactions near the cleavage site of the RNA template may help to further stabilize the nucleic acid at the RNase H active site and likely account, in part, for the increased rate of RNA cleavage observed for HIV-1 RT over XMRV RT (Fig. 1). Additional nucleic acid binding is provided for XMRV by the C helix (Fig. 8A), which is likely to provide additional interactions with the primer strand of the nucleic acid substrate.

We also compared the model of the XMRV ΔC RNase H-RNA-DNA complex with the previously determined crystal structure of *B. halodurans* in complex with an RNA-DNA substrate (PDB ID, 1ZBI; Fig. 8C) (62). The structure of *B. halodurans* shows a different mode of substrate binding (likely due to the presence of a second molecule on the same substrate) but demonstrates more similarities to the HIV-1 RNase H structure rather than the XMRV RNase H. Unlike XMRV (and HIV-1 when only one divalent metal is present in the active site) RNase H, the scissile phosphate on the RNA template in *B. halodurans* is stabilized by a second Mg^{2+} ion and not a histidine or any other residues from the enzyme. This Mg^{2+} ion is stabilized by Asp192, similar to the role of Asp549 in HIV-1 RNase H. Also similar to HIV-1 RNase H, the RNA template in *B. halodurans* is stabilized by a Gln at position 134 (Gln500 in HIV-1 RNase H). However, the Gln interacts with the base portion of the RNA template 3 bases in front of (toward the 5′ end of the template) the scissile phosphate instead of the phosphate backbone closer to the scissile phosphate. The RNA template in the *B. halodurans* structure is further stabilized by Ser74, Gly76 (neither of which appears in HIV-1 or XMRV RNase H), Asn105, and Asn106 (which correspond to Asn474 and Gln475 in HIV-1 RNase H, respectively).

Of the 18 amino acid differences (11%) between the XMRV and MoMLV ΔC RNase H domains, 4 appear in positions near the nucleic acid and therefore may affect substrate binding. Three residues (593, 594, and 609) are located in the RNase H primer grip, while one residue (528) is situated in β-sheet 1 near the active site and facing out toward the template strand of the nucleic acid. Residue 528 is likely to have the largest effect on substrate binding, as the change from Leu in MoMLV, which interacts with the nucleic acid, to Phe in XMRV, which points away from the RNA

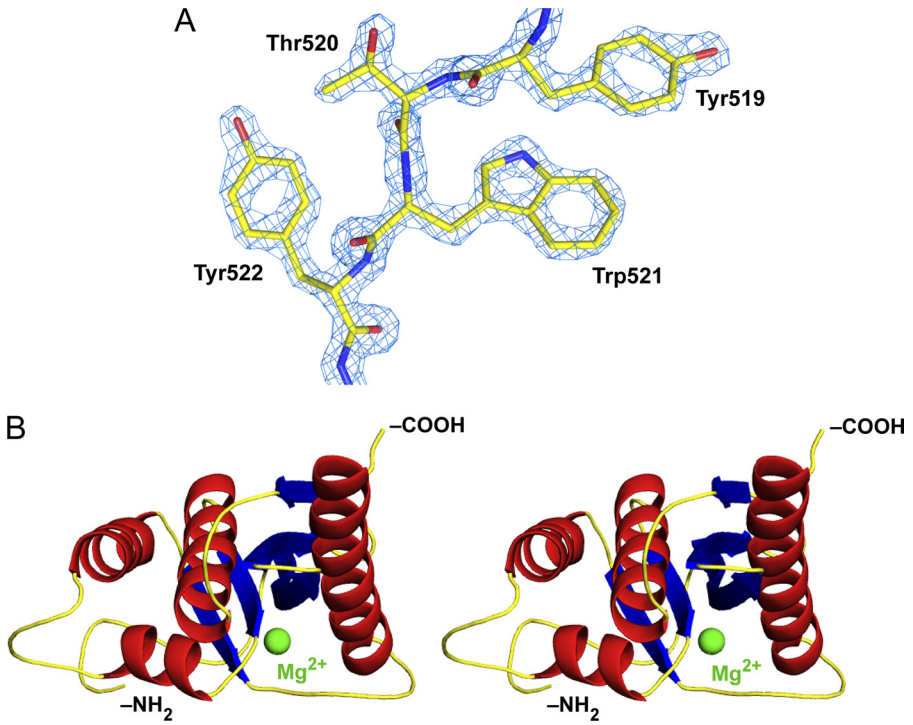

FIG 5 Crystal structure of the isolated XMRV ΔC RNase H domain. (A) $2F_o$-F_c electron density map of XMRV ΔC RNase H, displayed at $\sigma = 2.0$. (B) Stereo view of the isolated XMRV ΔC RNase H domain structure in cartoon representation. The structure contains an internal mixed β-sheet (shown in blue), composed of four parallel strands and one antiparallel strand, and four α-helices (shown in red). One Mg^{2+} ion (shown as a green sphere) is coordinated in the active site. Images were made using PyMOL (74).

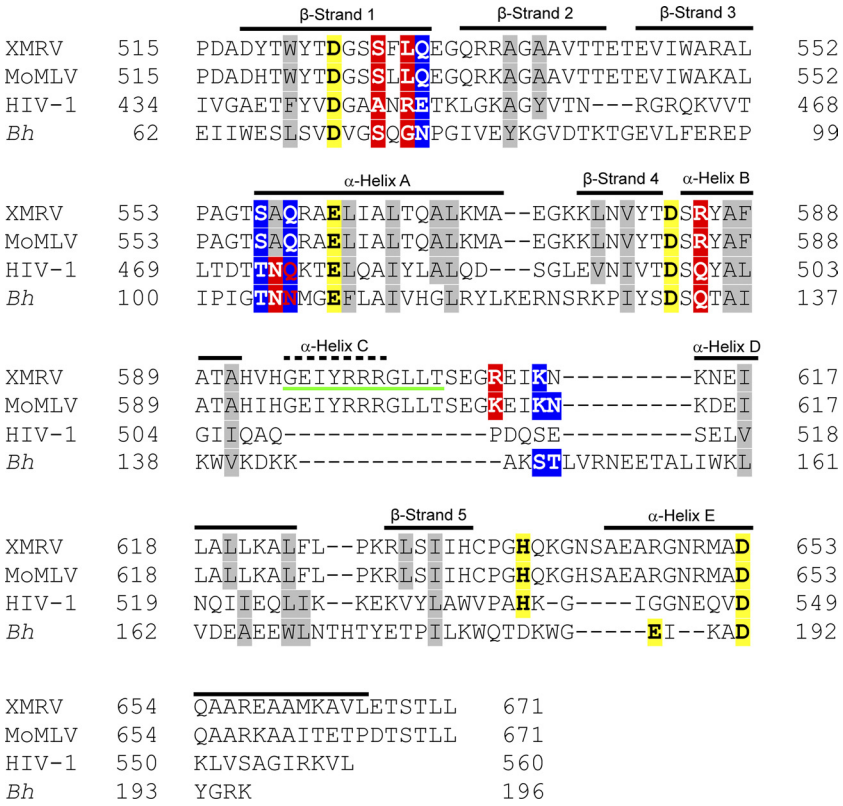

FIG 6 Sequence alignment of XMRV, MoMLV, HIV-1, and *B. halodurans* (*Bh*) RNases H. All deleted residues from the XMRV ΔC RNase H structure are underlined in green. Residues contacting the RNA template are highlighted in red, residues contacting the DNA primer are highlighted in blue and residues contacting both the RNA template and DNA primer are highlighted in blue with red letters. Hydrophobic core residues are highlighted in gray. Conserved active-site residues are highlighted in yellow.

template strand, possibly affects the stabilization of the nucleic acid near the RNase H active site. This may partially account for the lower rate of RNA cleavage observed for XMRV RT (0.32 min^{-1}) than for MoMLV RT (1.07 min^{-1}) in the presence of Mn^{2+} (Fig. 1).

DISCUSSION

The RNase H activity of retroviral RTs is critical for successful replication of the viral genome. In addition to the polymerase activity of RTs, which has historically been a popular target for antiretrovirals, the RNase H domain has also become an attractive target for antiviral therapies. A sound understanding of the function and structure of not only lentiviral but also gammaretroviral enzymes will aid in the design of novel, specific, and more potent inhibitors against retroviral RNase H function.

Our detailed analysis of the functional properties of gammaretroviral RNases H highlights similarities to and differences from the related lentiviral HIV-1 counterpart. XMRV and MoMLV RNases H are considerably less active than HIV-1 RNase H. This may be due to the weaker binding affinity of XMRV RT for the nucleic acid substrate (XMRV RT K_d > HIV-1 RT K_d), due to a rate of dissociation (k_{off}) that is higher than that of HIV-1 RT (61). Structural differences may also play a role in the observed decrease in RNase H activity for the gammaretroviral enzymes. Both the MoMLV and XMRV RTs exist as monomers, unlike the heterodimeric HIV-1 RT, which benefits from the additional support provided by the p51 subunit (17). An additional difference in nucleic acid binding includes the longer distance between the polymerase and RNase H active sites in XMRV RT than in HIV-1 RT (1 bp or approximately 3.4 Å) (28, 76). Such differences may affect the trajectory of the nucleic acid at the RNase H active site and the coordination of active site metals with the scissile phosphate group, thus explaining the difference in metal preference between the gammaretroviral (Mn^{2+}) and lentiviral (Mg^{2+}) RNases H.

Unlike the gammaretroviral RTs, HIV-1 RT lacks α-helix C in the RNase H domain, which is thought to be important for substrate binding (5, 26, 39, 51, 52), as the p15 RNase H domain of HIV-1 RT has no enzymatic activity (81, 82, 97). Addition of a highly basic loop from *E. coli* RNase H to the p15 HIV-1 RNase H fragment has been shown to enhance the RNase H activity of HIV-1 (41, 83).

RNHIs may offer expanded therapeutic options by complementing existing treatments. Some of these inhibitors were initially discovered as HIV-1 integrase inhibitors (85, 89) and were designed as active-site-directed compounds that would bind divalent metals at the integrase or RNase H active site (2, 8, 9, 21, 42, 87, 88). Acylhydrazone-based (11, 30, 35, 80), hydroxyisoquinolinedione-based (8, 9), and naphthyridinone-based (84, 95) compounds are three classes of HIV-1 RNHIs. Like most RNHIs, these compounds are based on metal-chelating pharmacophore scaffolds that have been optimized for potent inhibition of HIV-1 RNase H. Our data are consistent with previous results suggesting that naphthyridinone NAPHRHI binds to the RNase H active site of HIV-1 RT and extend these

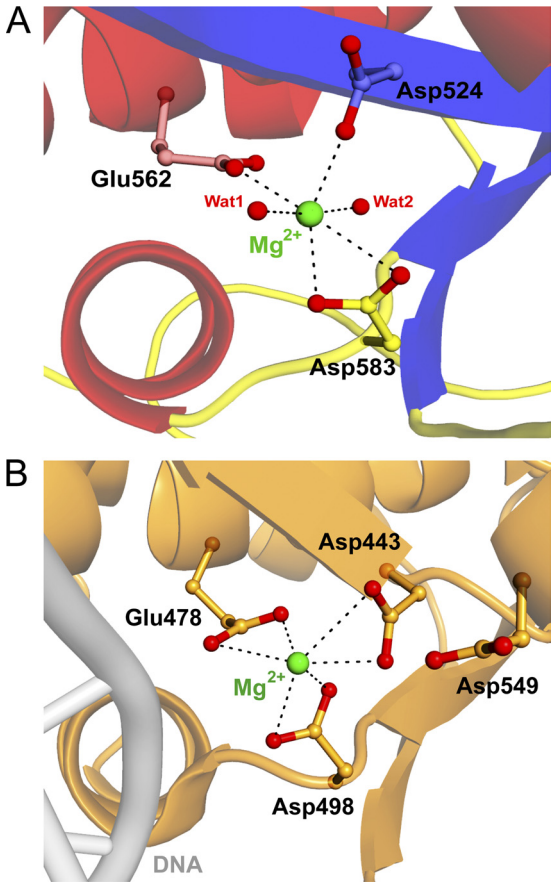

FIG 7 Comparison of the RNase H active sites of isolated XMRV RNase H ΔC and HIV-1 RT-dsDNA. (A) The active site of XMRV RNase H ΔC. One Mg^{2+} ion (green sphere) is coordinated by the conserved catalytic residues Asp524, Glu562, and Asp583 (shown as sticks) and two water molecules (red spheres [Wat1 and Wat2]). (B) The RNase H active site of HIV-1 RT-dsDNA (PDB ID, 3KJV). One Mg^{2+} ion (green sphere) is coordinated by the conserved catalytic residues Asp443, Glu478, and Asp498 (shown as sticks). The other conserved active-site residue, Asp549, is also shown. The dsDNA is shown in light gray. Images were made using PyMOL (74).

findings for XMRV RNase H (95). Interestingly, unlike the hydroxytropolone β-thujaplicinol, which can inhibit HIV-1 RNase H only when added to the reaction mixture before the nucleic acid substrate (6), NAPHRHI can access the RNase H active site even in the presence of RNA-DNA, especially in the presence of Mn^{2+} (Fig. 4B and C). Furthermore, in the presence of Mg^{2+}, NAPHRHI is less effective against both XMRV RT and isolated RNase H. This suggests that Mn^{2+} binds NAPHRHI more tightly than Mg^{2+}, thus making NAPHRHI a more effective inhibitor in the presence of Mn^{2+}. Additional data show that, unlike the potency of β-thujaplicinol, the concentration of the RNA-DNA substrate does not decrease that of NAPHRHI (Table 2), and therefore, the inhibitor does not compete with the nucleic acid substrate for binding to the enzyme. Our data also demonstrate that NAPHRHI inhibited the DNA polymerase activities of XMRV and HIV-1 RTs significantly less efficiently (>50-fold) than the corresponding RNase H activities. Moreover, the inhibitor efficiently blocked the RNase H function of the XMRV and p15-Ec HIV-1 RNase H fragments. Therefore, the primary mechanism of RNase H inhibition by NAPHRHI is targeting of the RNase H active site (95).

The hydroxyisoquinolinedione compound YLC2-155 was a potent RNHI of both HIV-1 RT and p15-Ec RNase H and a considerably less efficient inhibitor of the DNA polymerase activity of the RT. Interestingly, while YLC2-155 was also a potent RNHI of XMRV RT, it did not inhibit the DNA polymerase of XMRV RT and was also ineffective against the isolated XMRV RNase H domain. These data suggest that this compound may not bind at the RNase H or polymerase active site of XMRV RT. Instead, it may target a distinct binding site that allows inhibition of the RNase H and not of the DNA polymerase function. Collectively, our data demonstrate that RNHIs can specifically block RNase H function and could thus be further modified to enhance binding potency and selectivity.

Many RNHIs have been found to be potent against HIV-1 RT *in vitro* but exhibit little to no anti-HIV activity in cell-based assays (47). Similar to previous investigators, we found that NAPHRHI inhibits the RNase H function of HIV-1 RT (95). We also found that this compound inhibits the RNase H activity of the p15-Ec RNase H fragment. In addition, we showed that NAPHRHI blocks the replication of HIV in both pseudotype- and cell-based assays. The compound also appeared to have some antiviral activity against XMRV and MoMLV, but because the respective EC_{50}s were close to the CC_{50} (4.1 μM), it was not possible to accurately determine its potency against these viruses. These results suggest that the naphthyridinone scaffold is a promising candidate for future studies that will focus on identifying potent inhibitors of RNase H activity that are less toxic. Similarly, the acylhydrazone (BHMP07 and THBNH) and hydroxyisoquinolinedione (YLC2-155) compounds exhibit antiviral activity in cell-based assays but demonstrate low cytotoxic effects. Hence, further development of potent RNHIs based on the acylhydrazone and hydroxyisoquinolinedione scaffolds should be pursued.

In order to determine how the structure of XMRV RNase H might affect its function and inhibition, we determined the crystal structure of the XMRV ΔC RNase H fragment. Our data show extensive similarity between the XMRV and MoMLV ΔC RNase H structures (RMSD, 0.39 Å), consistent with their high sequence identity (61). The active site of XMRV RNase H is also similar to that of HIV-1 RNase H (RMSD, 1.6 Å). The catalytic residues (Asp524, Glu562, and Asp583) of XMRV RNase H correspond to residues Asp443, Glu478, and Asp498 of HIV-1 RNase H (Fig. 7B). An additional HIV-1 RNase H residue, Asp549 (Asp653 in XMRV RNase H), also participates in RNase H cleavage by helping to stabilize one of the catalytic metals (5). Many crystal structures of HIV-1 RT and RNase H show a single Mg^{2+} ion in the RNase H active site (37, 48, 92). However, recent structures of HIV-1 RT and isolated RNase H with active-site-directed RNHIs show two Mn^{2+} ions in the RNase H active site (47, 84). In addition, crystal structures of *B. halodurans* and human RNases H have also revealed two active-site Mg^{2+} ions (62, 63). Biochemical studies have also suggested a two-metal mechanism for the RNase H activity of RTs (44, 96). Interestingly, the XMRV and MoMLV ΔC RNase H structures contain a single metal at the active site. However, given the degree of similarity with the HIV-1 RT, it is likely that RNase H cleavage or binding of RNHI would also involve two divalent metals.

In conclusion, we have determined the differences in RNase H activity and the effectiveness of acylhydrazone-, naphthyridinone-,

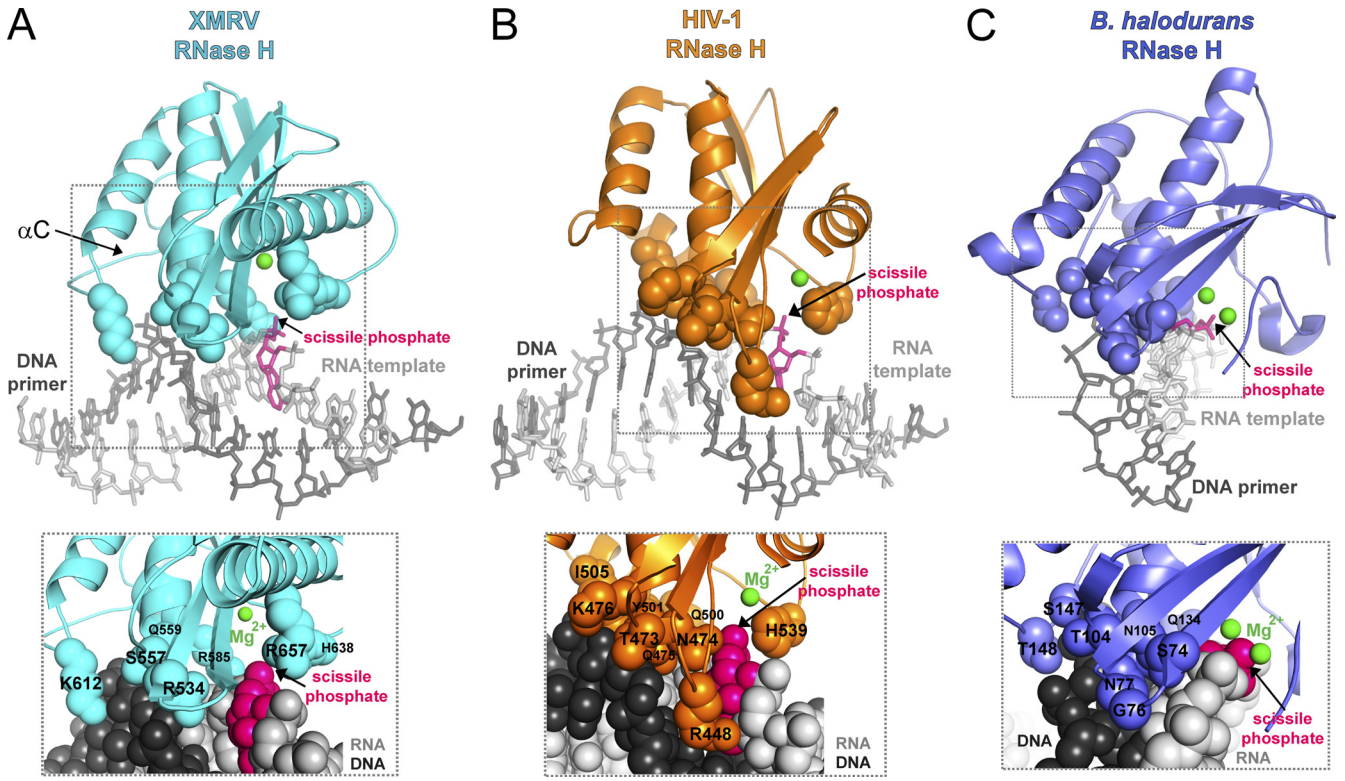

FIG 8 Interactions of RNases H with RNA-DNA substrates. (A) Molecular model showing potential interactions of XMRV ΔC RNase H (cyan cartoon) with an RNA-DNA substrate. The molecular model was built using the crystallographic coordinates of unliganded XMRV ΔC RNase H and an RNA-DNA oligonucleotide as described in Materials and Methods. The location of helix C (which would contact the primer strand) is shown by the arrow. (B) Cartoon representation of the HIV-1 RNase H complex with a polypurine tract RNA-DNA substrate (1HYS, orange cartoon). (C) Cartoon representation of the *B. halodurans* RNase H complex with an RNA-DNA substrate (1ZBI, blue cartoon). The RNA templates are shown as light gray sticks and spheres, while the DNA primers are shown as dark gray sticks and spheres. RNase H residues that interact with the nucleic acid are shown as space-filling spheres in their respective colors. Locations of the Mg^{2+} ions are shown as green spheres, and the RNA base containing the scissile phosphate is shown in pink. Images were made using PyMOL (74).

and hydroxyisoquinolinedione-based RNHIs against gammaretroviral and lentiviral RTs. The crystal structure of the isolated XMRV RNase H domain provides a structural framework for better understanding the function and inhibition of gammaretroviral RNase H activity. This information may be useful in the design of next-generation RNHIs with increased potency against retroviral RTs.

ACKNOWLEDGMENTS

This work was supported in part by NIH grants AI076119, AI094715, and AI074389 to S.G.S. and AI073975 and AI077424 to M.A.P. We also acknowledge support by a grant from the Ministry of Knowledge and Economy, Bilateral International Collaborative R&D Program, Republic of Korea. B.M. was the recipient of an amfAR Mathilde Krim Fellowship and a Canadian Institutes of Health Research (CIHR) fellowship.

REFERENCES

1. **Adams PD, et al.** 2002. PHENIX: building new software for automated crystallographic structure determination. Acta Crystallogr. D Biol. Crystallogr. **58**:1948–1954.
2. **Andréola ML, et al.** 2002. HIV-1 integrase and RNase H activities as therapeutic targets. Expert Opin. Ther. Targets **6**:433–446.
3. **Balzarini J, et al.** 1994. Human immunodeficiency virus 1 (HIV-1)-specific reverse transcriptase (RT) inhibitors may suppress the replication of specific drug-resistant (E138K)RT HIV-1 mutants or select for highly resistant (Y181C→C181I)RT HIV-1 mutants. Proc. Natl. Acad. Sci. U. S. A. **91**:6599–6603.
4. **Bauman JD, et al.** 2008. Crystal engineering of HIV-1 reverse transcriptase for structure-based drug design. Nucleic Acids Res. **36**:5083–5092.
5. **Beilhartz GL, Gotte M.** 2010. HIV-1 ribonuclease H: structure, catalytic mechanism and inhibitors. Viruses **2**:900–926.
6. **Beilhartz GL, et al.** 2009. HIV-1 reverse transcriptase can simultaneously engage its DNA/RNA substrate at both DNA polymerase and RNase H active sites: implications for RNase H inhibition. J. Mol. Biol. **388**:462–474.
7. **Biaglow JE, Kachur AV.** 1997. The generation of hydroxyl radicals in the reaction of molecular oxygen with polyphosphate complexes of ferrous ion. Radiat. Res. **148**:181–187.
8. **Billamboz M, et al.** 2008. Design, synthesis, and biological evaluation of a series of 2-hydroxyisoquinoline-1,3(2H,4H)-diones as dual inhibitors of human immunodeficiency virus type 1 integrase and the reverse transcriptase RNase H domain. J. Med. Chem. **51**:7717–7730.
9. **Billamboz M, et al.** 2011. Magnesium chelating 2-hydroxyisoquinoline-1,3(2H,4H)-diones, as inhibitors of HIV-1 integrase and/or the HIV-1 reverse transcriptase ribonuclease H domain: discovery of a novel selective inhibitor of the ribonuclease H function. J. Med. Chem. **54**:1812–1824.
10. **Bokesch HR, et al.** 2008. HIV-1 ribonuclease H inhibitory phenolic glycosides from Eugenia hyemalis. J. Nat. Prod. **71**:1634–1636.
11. **Borkow G, et al.** 1997. Inhibition of the ribonuclease H and DNA polymerase activities of HIV-1 reverse transcriptase by *N*-(4-*tert*-butylbenzoyl)-2-hydroxy-1-naphthaldehyde hydrazone. Biochemistry **36**:3179–3185.
12. **Budihas SR, et al.** 2005. Selective inhibition of HIV-1 reverse transcriptase-associated ribonuclease H activity by hydroxylated tropolones. Nucleic Acids Res. **33**:1249–1256.
13. **Chen YL, et al.** 2012. The design, synthesis and biological evaluations of C-6 or C-7 substituted 2-hydroxyisoquinoline-1,3-diones as inhibitors of hepatitis C virus. Bioorg. Med. Chem. **20**:467–479.
14. **Chowdhury K, Kaushik N, Pandey VN, Modak MJ.** 1996. Elucidation of

the role of Arg 110 of murine leukemia virus reverse transcriptase in the catalytic mechanism: biochemical characterization of its mutant enzymes. Biochemistry **35**:16610–16620.
15. **Chung S, et al.** 2011. Synthesis, activity, and structural analysis of novel α-hydroxytropolone inhibitors of human immunodeficiency virus reverse transcriptase-associated ribonuclease H. J. Med. Chem. **54**:4462–4473.
16. **Chung S, et al.** 2010. Structure-activity analysis of vinylogous urea inhibitors of human immunodeficiency virus-encoded ribonuclease H. Antimicrob. Agents Chemother. **54**:3913–3921.
17. **Coté ML, Roth MJ.** 2008. Murine leukemia virus reverse transcriptase: structural comparison with HIV-1 reverse transcriptase. Virus Res. **134**: 186–202.
18. **Das D, Georgiadis MM.** 2004. The crystal structure of the monomeric reverse transcriptase from Moloney murine leukemia virus. Structure **12**: 819–829.
19. **Dat NT, et al.** 2007. A dimeric lactone from Ardisia japonica with inhibitory activity for HIV-1 and HIV-2 ribonuclease H. J. Nat. Prod. **70**:839–841.
20. **Davis IW, et al.** 2007. MolProbity: all-atom contacts and structure validation for proteins and nucleic acids. Nucleic Acids Res. **35**:W375–W383.
21. **Didierjean J, et al.** 2005. Inhibition of human immunodeficiency virus type 1 reverse transcriptase, RNase H, and integrase activities by hydroxytropolones. Antimicrob. Agents Chemother. **49**:4884–4894.
22. **Durk RC, et al.** 2010. Inhibitors of foot and mouth disease virus targeting a novel pocket of the RNA-dependent RNA polymerase. PLoS One **5**:e15049.
23. **Edward JT, Gauthier M, Chubb FL, Ponka P.** 1988. Synthesis of new acylhydrazones as iron-chelating compounds. J. Chem. Eng. Data **33**:538–540.
24. **Ehteshami M, et al.** 2008. Connection domain mutations N348I and A360V in HIV-1 reverse transcriptase enhance resistance to 3′-azido-3′-deoxythymidine through both RNase H-dependent and -independent mechanisms. J. Biol. Chem. **283**:22222–22232.
25. **Emsley P, Cowtan K.** 2004. Coot: model-building tools for molecular graphics. Acta Crystallogr. D Biol. Crystallogr. **60**:2126–2132.
26. **Farias RV, et al.** 2011. Expression of an Mg^{2+}-dependent HIV-1 RNase H construct for drug screening. Antimicrob. Agents Chemother. **55**:4735–4741.
27. **Fuji H, et al.** 2009. Derivatives of 5-nitro-furan-2-carboxylic acid carbamoylmethyl ester inhibit RNase H activity associated with HIV-1 reverse transcriptase. J. Med. Chem. **52**:1380–1387.
28. **Gao HQ, Sarafianos SG, Arnold E, Hughes SH.** 1999. Similarities and differences in the RNase H activities of human immunodeficiency virus type 1 reverse transcriptase and Moloney murine leukemia virus reverse transcriptase. J. Mol. Biol. **294**:1097–1113.
29. **Georgiadis MM, et al.** 1995. Mechanistic implications from the structure of a catalytic fragment of Moloney murine leukemia virus reverse transcriptase. Structure **3**:879–892.
30. **Gong Q, et al.** 2011. Interaction of HIV-1 reverse transcriptase ribonuclease H with an acylhydrazone inhibitor. Chem. Biol. Drug Des. **77**:39–47.
31. **Hachiya A, et al.** 2001. Rapid and simple phenotypic assay for drug susceptibility of human immunodeficiency virus type 1 using CCR5-expressing HeLa/CD4(+) cell clone 1–10 (MAGIC-5). Antimicrob. Agents Chemother. **45**:495–501.
32. **Hachiya A, et al.** 2011. K70Q adds high-level tenofovir resistance to "Q151M complex" HIV reverse transcriptase through the enhanced discrimination mechanism. PLoS One **6**:e16242.
33. **Hang JQ, et al.** 2004. Activity of the isolated HIV RNase H domain and specific inhibition by N-hydroxyimides. Biochem. Biophys. Res. Commun. **317**:321–329.
34. **Himmel DM, et al.** 2009. Structure of HIV-1 reverse transcriptase with the inhibitor beta-thujaplicinol bound at the RNase H active site. Structure **17**:1625–1635.
35. **Himmel DM, et al.** 2006. HIV-1 reverse transcriptase structure with RNase H inhibitor dihydroxy benzoyl naphthyl hydrazone bound at a novel site. ACS Chem. Biol. **1**:702–712.
36. **Hossain MM, Parniak MA.** 2006. In vitro microbicidal activity of the nonnucleoside reverse transcriptase inhibitor (NNRTI) UC781 against NNRTI-resistant human immunodeficiency virus type 1. J. Virol. **80**: 4440–4446.
37. **Huang H, Chopra R, Verdine GL, Harrison SC.** 1998. Structure of a covalently trapped catalytic complex of HIV-1 reverse transcriptase: implications for drug resistance. Science **282**:1669–1675.
38. **Jacobo-Molina A, et al.** 1993. Crystal structure of human immunodeficiency virus type 1 reverse transcriptase complexed with double-stranded DNA at 3.0 A resolution shows bent DNA. Proc. Natl. Acad. Sci. U. S. A. **90**:6320–6324.
39. **Kanaya S, Katsuda-Nakai C, Ikehara M.** 1991. Importance of the positive charge cluster in Escherichia coli ribonuclease HI for the effective binding of the substrate. J. Biol. Chem. **266**:11621–11627.
40. **Kaushik N, Chowdhury K, Pandey VN, Modak MJ.** 2000. Valine of the YVDD motif of Moloney murine leukemia virus reverse transcriptase: role in the fidelity of DNA synthesis. Biochemistry **39**:5155–5165.
41. **Keck JL, Marqusee S.** 1995. Substitution of a highly basic helix/loop sequence into the RNase H domain of human immunodeficiency virus reverse transcriptase restores its Mn(2+)-dependent RNase H activity. Proc. Natl. Acad. Sci. U. S. A. **92**:2740–2744.
42. **Kirschberg T, Parrish J.** 2007. Metal chelators as antiviral agents. Curr. Opin. Drug Discov Devel. **10**:460–472.
43. **Kirschberg TA, et al.** 2009. RNase H active site inhibitors of human immunodeficiency virus type 1 reverse transcriptase: design, biochemical activity, and structural information. J. Med. Chem. **52**:5781–5784.
44. **Klumpp K, et al.** 2003. Two-metal ion mechanism of RNA cleavage by HIV RNase H and mechanism-based design of selective HIV RNase H inhibitors. Nucleic Acids Res. **31**:6852–6859.
45. **Kohlstaedt LA, Wang J, Friedman JM, Rice PA, Steitz TA.** 1992. Crystal structure at 3.5 A resolution of HIV-1 reverse transcriptase complexed with an inhibitor. Science **256**:1783–1790.
46. **Langer G, Cohen SX, Lamzin VS, Perrakis A.** 2008. Automated macromolecular model building for X-ray crystallography using ARP/wARP version 7. Nat. Protoc. **3**:1171–1179.
47. **Lansdon EB, et al.** 2011. Structural and binding analysis of pyrimidinol carboxylic acid and N-hydroxy quinazolinedione HIV-1 RNase H inhibitors. Antimicrob. Agents Chemother. **55**:2905–2915.
48. **Lansdon EB, et al.** 2010. Visualizing the molecular interactions of a nucleotide analog, GS-9148, with HIV-1 reverse transcriptase-DNA complex. J. Mol. Biol. **397**:967–978.
49. **Larder BA, Kemp SD.** 1989. Multiple mutations in HIV-1 reverse transcriptase confer high-level resistance to zidovudine (AZT). Science **246**: 1155–1158.
50. **Le Grice SFJ.** 1993. Reverse transcriptase. Cold Spring Harbor Laboratory Press, Plainview, NY.
51. **Lim D, et al.** 2006. Crystal structure of the Moloney murine leukemia virus RNase H domain. J. Virol. **80**:8379–8389.
52. **Lim D, Orlova M, Goff SP.** 2002. Mutations of the RNase H C helix of the Moloney murine leukemia virus reverse transcriptase reveal defects in polypurine tract recognition. J. Virol. **76**:8360–8373.
53. **Marchand B, Gotte M.** 2003. Site-specific footprinting reveals differences in the translocation status of HIV-1 reverse transcriptase. Implications for polymerase translocation and drug resistance. J. Biol. Chem. **278**:35362–35372.
54. **Matthews BW.** 1985. Determination of protein molecular weight, hydration, and packing from crystal density. Methods Enzymol. **114**:176–187.
55. **McCoy AJ, et al.** 2007. Phaser crystallographic software. J. Appl. Crystallogr. **40**:658–674.
56. **Michailidis E, et al.** 2009. Mechanism of inhibition of HIV-1 reverse transcriptase by 4′-ethynyl-2-fluoro-2′-deoxyadenosine triphosphate, a translocation-defective reverse transcriptase inhibitor. J. Biol. Chem. **284**: 35681–35691.
57. **Mooij WT, Cohen SX, Joosten K, Murshudov GN, Perrakis A.** 2009. "Conditional restraints": restraining the free atoms in ARP/wARP. Structure **17**:183–189.
58. **Mulky A, Sarafianos SG, Arnold E, Wu X, Kappes JC.** 2004. Subunit-specific analysis of the human immunodeficiency virus type 1 reverse transcriptase in vivo. J. Virol. **78**:7089–7096.
59. **Murshudov GN, Vagin AA, Dodson EJ.** 1997. Refinement of macromolecular structures by the maximum-likelihood method. Acta Crystallogr. D Biol. Crystallogr. **53**:240–255.
60. **Najmudin S, et al.** 2000. Crystal structures of an N-terminal fragment from Moloney murine leukemia virus reverse transcriptase complexed with nucleic acid: functional implications for template-primer binding to the fingers domain. J. Mol. Biol. **296**:613–632.
61. **Ndongwe TP, et al.** 2012. Biochemical, inhibition and inhibitor resistance

studies of xenotropic murine leukemia virus-related virus reverse transcriptase. Nucleic Acids Res. **40**:345–359.
62. **Nowotny M, Gaidamakov SA, Crouch RJ, Yang W.** 2005. Crystal structures of RNase H bound to an RNA/DNA hybrid: substrate specificity and metal-dependent catalysis. Cell **121**:1005–1016.
63. **Nowotny M, et al.** 2007. Structure of human RNase H1 complexed with an RNA/DNA hybrid: insight into HIV reverse transcription. Mol. Cell **28**:264–276.
64. **Paprotka T, et al.** 2010. Inhibition of xenotropic murine leukemia virus-related virus by APOBEC3 proteins and antiviral drugs. J. Virol. **84**:5719–5729.
65. **Parniak MA, Min KL, Budihas SR, Le Grice SF, Beutler JA.** 2003. A fluorescence-based high-throughput screening assay for inhibitors of human immunodeficiency virus-1 reverse transcriptase-associated ribonuclease H activity. Anal. Biochem. **322**:33–39.
66. **Perrakis A, Harkiolaki M, Wilson KS, Lamzin VS.** 2001. ARP/wARP and molecular replacement. Acta Crystallogr. D Biol. Crystallogr. **57**:1445–1450.
67. **Pflugrath JW.** 1999. The finer things in X-ray diffraction data collection. Acta Crystallogr. D Biol. Crystallogr. **55**:1718–1725.
68. **Richman DD.** 1993. HIV drug resistance. Annu. Rev. Pharmacol. Toxicol. **33**:149–164.
69. **Sarafianos SG, et al.** 2002. Structures of HIV-1 reverse transcriptase with pre- and post-translocation AZTMP-terminated DNA. EMBO J. **21**:6614–6624.
70. **Sarafianos SG, et al.** 2003. Trapping HIV-1 reverse transcriptase before and after translocation on DNA. J. Biol. Chem. **278**:16280–16288.
71. **Sarafianos SG, et al.** 2001. Crystal structure of HIV-1 reverse transcriptase in complex with a polypurine tract RNA:DNA. EMBO J. **20**:1449–1461.
72. **Sarafianos SG, et al.** 2009. Structure and function of HIV-1 reverse transcriptase: molecular mechanisms of polymerization and inhibition. J. Mol. Biol. **385**:693–713.
73. **Schinazi RF, et al.** 1993. Characterization of human immunodeficiency viruses resistant to oxathiolane-cytosine nucleosides. Antimicrob. Agents Chemother. **37**:875–881.
74. **Schrödinger L.** 2010. The PyMOL molecular graphics system, version 1.3. Schrödinger, LLC, Mannheim, Germany.
75. **Schuckmann MM, et al.** 2010. The N348I mutation at the connection subdomain of HIV-1 reverse transcriptase decreases binding to nevirapine. J. Biol. Chem. **285**:38700–38709.
76. **Schultz SJ, Zhang M, Champoux JJ.** 2010. Multiple nucleotide preferences determine cleavage-site recognition by the HIV-1 and M-MuLV RNases H. J. Mol. Biol. **397**:161–178.
77. **Shaw-Reid CA, et al.** 2005. Dissecting the effects of DNA polymerase and ribonuclease H inhibitor combinations on HIV-1 reverse-transcriptase activities. Biochemistry **44**:1595–1606.
78. **Shaw-Reid CA, et al.** 2003. Inhibition of HIV-1 ribonuclease H by a novel diketo acid, 4-[5-(benzoylamino)thien-2-yl]-2,4-dioxobutanoic acid. J. Biol. Chem. **278**:2777–2780.
79. **Singh K, Marchand B, Kirby KA, Michailidis E, Sarafianos SG.** 2010. Structural aspects of drug resistance and inhibition of HIV-1 reverse transcriptase. Viruses **2**:606–638.
80. **Sluis-Cremer N, Arion D, Parniak MA.** 2002. Destabilization of the HIV-1 reverse transcriptase dimer upon interaction with N-acyl hydrazone inhibitors. Mol. Pharmacol. **62**:398–405.
81. **Smith JS, Gritsman K, Roth MJ.** 1994. Contributions of DNA polymerase subdomains to the RNase H activity of human immunodeficiency virus type 1 reverse transcriptase. J. Virol. **68**:5721–5729.
82. **Smith JS, Roth MJ.** 1993. Purification and characterization of an active human immunodeficiency virus type 1 RNase H domain. J. Virol. **67**:4037–4049.
83. **Stahl SJ, Kaufman JD, Vikic-Topic S, Crouch RJ, Wingfield PT.** 1994. Construction of an enzymatically active ribonuclease H domain of human immunodeficiency virus type 1 reverse transcriptase. Protein Eng. **7**:1103–1108.
84. **Su HP, et al.** 2010. Structural basis for the inhibition of RNase H activity of HIV-1 reverse transcriptase by RNase H active site-directed inhibitors. J. Virol. **84**:7625–7633.
85. **Summa V, et al.** 2006. 4,5-Dihydroxypyrimidine carboxamides and *N*-alkyl-5-hydroxypyrimidinone carboxamides are potent, selective HIV integrase inhibitors with good pharmacokinetic profiles in preclinical species. J. Med. Chem. **49**:6646–6649.
86. **Takada K, et al.** 2007. An HIV RNase H inhibitory 1,3,4,5-tetragalloylapiitol from the African plant Hylodendron gabunensis. J. Nat. Prod. **70**:1647–1649.
87. **Tang J, et al.** 2011. 6-Benzoyl-3-hydroxypyrimidine-2,4-diones as dual inhibitors of HIV reverse transcriptase and integrase. Bioorg. Med. Chem. Lett. **21**:2400–2402.
88. **Tang J, et al.** 2011. N-3 hydroxylation of pyrimidine-2,4-diones yields dual inhibitors of HIV reverse transcriptase and integrase. ACS Med. Chem. Lett. **2**:63–67.
89. **Tang J, et al.** 2011. 3-Hydroxypyrimidine-2,4-diones as an inhibitor scaffold of HIV integrase. J. Med. Chem. **54**:2282–2292.
90. **Telesnitsky A, Goff SP.** 1993. RNase H domain mutations affect the interaction between Moloney murine leukemia virus reverse transcriptase and its primer-template. Proc. Natl. Acad. Sci. U. S. A. **90**:1276–1280.
91. **Tramontano E, et al.** 2005. 6-[1-(4-Fluorophenyl)methyl-1H-pyrrol-2-yl)]-2,4-dioxo-5-hexenoic acid ethyl ester a novel diketo acid derivative which selectively inhibits the HIV-1 viral replication in cell culture and the ribonuclease H activity in vitro. Antiviral Res. **65**:117–124.
92. **Tu X, et al.** 2010. Structural basis of HIV-1 resistance to AZT by excision. Nat. Struct. Mol. Biol. **17**:1202–1209.
93. **Tuske S, et al.** 2004. Structures of HIV-1 RT-DNA complexes before and after incorporation of the anti-AIDS drug tenofovir. Nat. Struct. Mol. Biol. **11**:469–474.
94. **Wendeler M, et al.** 2008. Vinylogous ureas as a novel class of inhibitors of reverse transcriptase-associated ribonuclease H activity. ACS Chem. Biol. **3**:635–644.
95. **Williams PD, et al.** 2010. Potent and selective HIV-1 ribonuclease H inhibitors based on a 1-hydroxy-1,8-naphthyridin-2(1H)-one scaffold. Bioorg. Med. Chem. Lett. **20**:6754–6757.
96. **Yang W, Lee JY, Nowotny M.** 2006. Making and breaking nucleic acids: two-Mg^{2+}-ion catalysis and substrate specificity. Mol. Cell **22**:5–13.
97. **Zúñiga R, Sengupta S, Snyder C, Leon O, Roth MJ.** 2004. Expression of the C terminus of HIV-1 reverse transcriptase p66 and p51 subunits as a single polypeptide with RNase H activity. Protein Eng. Des Sel. **17**:581–587.